Engineered Science
DOI: https://dx.doi.org/10.30919/es1508

Developing a Drone-Based Machine Learning for Spatial Modeling and Analysis of Biomass and Carbon Sequestration in Forest Ecosystems

Thinnakon Angkahad,[1] Teerawong Laosuwan,[1, 4,*] Satith Sangpradid,[2, 4,*] Narueset Prasertsri,[2] Yannawut Uttaruk,[3, 4] Titipong Phoophathong[1, 4] and Joe Nuchthapho[5]

Abstract

This study aims to utilize drones and machine learning for spatial modeling and analysis of biomass and carbon storage in forest ecosystems. The research utilizes Red Green Blue (RGB) imagery captured by drones as a tool for data analysis, employing Agisoft PhotoScan software to process data in conjunction with field measurements to create models for estimating above-ground biomass (AGB) and carbon storage. The machine learning techniques applied include Canopy Height Model (CHM) and Segment Mean Shift (SMS). The findings reveal that field data surveys identified a total of 1,241 tree species, with an estimated carbon storage of 213.53 tonnes of CO_2 equivalent (tCO_2e). Results from machine learning using the CHM technique showed a carbon storage estimation of 212.51 tCO_2e, with an error margin of 0.48% and a carbon storage difference of 1.01 tCO_2e. Meanwhile, the SMS technique estimated carbon storage at 207.01 tCO_2e, with an error margin of 3.15% and a carbon storage difference of 6.52 tCO_2e. It can be concluded that the CHM technique demonstrates higher accuracy compared to SMS in estimating carbon density. Additionally, further analysis of CHM results showed an accuracy of 0.597, precision of 0.902, recall of 0.638, an F1-score of 0.747, and an overall accuracy of 74.737%.

Keywords: Drones; Machine learning; Allometric equations; RGB imagery; Above ground biomass; Carbon sequestrations.
Received: 09 February 2025; Revised: 06 April 2025; Accepted: 04 May 2025.
Article type: Research article.

1. Introduction

Global warming refers to the increase in the average temperature of the Earth's atmosphere, affecting both the air near the Earth's surface and the ocean waters. This occurrence is attributed to the release of greenhouse gases resulting from human activities, including industrial operations, agricultural practices, and deforestation. Carbon dioxide (CO_2) is the most prevalent of these gases. The Revised 1996 IPCC Guidelines classify greenhouse gas emissions into six primary categories: (1) energy production, (2) industrial activities, (3) the use of solvents and products, (4) agricultural practices, (5) changes in land use and forestry, and (6) waste management. Each of these categories plays a substantial role in the rising levels of greenhouse gases in the atmosphere.[1-4] Furthermore, the 2014 assessment by the Intergovernmental Panel on Climate Change (IPCC) revealed that the past three decades have witnessed a continuous rise in global surface temperatures, with the period from 1983 to 2012 being the warmest 30 years in the past 1,400 years in the Northern Hemisphere. Carbon dioxide exhibited the most significant increase, accounting for approximately 67%, primarily due to the use of fossil fuels.[5] Additionally, deforestation contributes to approximately 20% of the increase in atmospheric carbon dioxide, resulting from the loss of carbon stored in wood biomass.[6]

The carbon cycle is the process by which carbon circulates throughout the environment in both organic and inorganic forms. This cycle plays a crucial role in maintaining environmental balance, particularly in regulating the Earth's

[1] *Department of Physics, Faculty of Science, Mahasarakham University, Maha Sarakham, 44150, Thailand*
[2] *Department of Geoinformatics, Faculty of Informatics, Mahasarakham University, Maha Sarakham, 44150, Thailand*
[3] *Department of Biology, Faculty of Science, Mahasarakham University, Maha Sarakham, 44150, Thailand*
[4] *Greenhouse Gas Research Center and Operations, Mahasarakham University, Maha Sarakham, 44150, Thailand*
[5] *Murdoch Children's Research Institute, 50 Flemington Road, Parkville, Victoria 3052, Australia*
**Email:* teerawong@msu.ac.th (T. Laosuwan); satith.s@msu.ac.th (S. Sangpradid)

climate.[7] Changes in the carbon cycle, such as the rise in atmospheric carbon dioxide from human activities, are key factors contributing to global warming and climate change.[8,9] Trees play a vital role as carbon sinks, absorbing carbon from the atmosphere through photosynthesis. The absorbed carbon is stored as tree biomass. A decline in forested areas reduces carbon storage capacity and releases carbon stored in trees back into the atmosphere. This release significantly contributes to the greenhouse effect and global warming. Therefore, accurate data on forest carbon storage is critical for planning strategies to reduce greenhouse gas concentrations in the atmosphere.[10-13] In general, the amount of carbon stored in trees is directly related to biomass, which includes the total mass of all tree components: stems, branches, leaves, and roots. Anatomical characteristics of trees, such as height, trunk size, and crown width, can be used to estimate the amount of carbon stored in trees through the use of allometric equations. These equations represent the relationship between biomass and tree structure and are valuable tools for studying carbon storage in forest ecosystems.[14-18]

In examining the structural attributes of trees, data can be collected through field surveys. Although these surveys yield precise information regarding tree structures and forms, they necessitate the involvement of specialized personnel and demand considerable time and financial investment.[19-21] This is especially relevant in scenarios where the study area is characterized by dense natural vegetation and is situated at a considerable distance from human habitation, rendering field surveys difficult and increasing the likelihood of data collection inaccuracies.[22-24] Currently, remote sensing technology has advanced significantly, particularly in the field of high-resolution satellite imagery and aerial imagery captured by drones, including RGB and multispectral formats. These technologies can be effectively applied to study the structural characteristics and density of natural vegetation in forested areas.[25-27] Additionally, they can be employed to more accurately assess the quantity of carbon sequestered in forested regions.[28-30] Utilizing RGB imagery captured by drones to investigate carbon storage in community forests presents a fascinating methodology. The research team intends to leverage data obtained from drones to assess the carbon storage capabilities in regions characterized by relatively uncomplicated vegetation structures and biophysical traits. This study will provide essential baseline data for analysis and comparisons with areas that have more complex vegetation structures. Furthermore, it may enhance the understanding of carbon storage processes in various ecosystems, such as tropical evergreen forests and mixed deciduous forests.

2. Materials and methods

2.1 Study area

The study area is a community forest situated in Tha Song Khon Subdistrict, Mueang Maha Sarakham District, Maha Sarakham Province (Fig. 1).

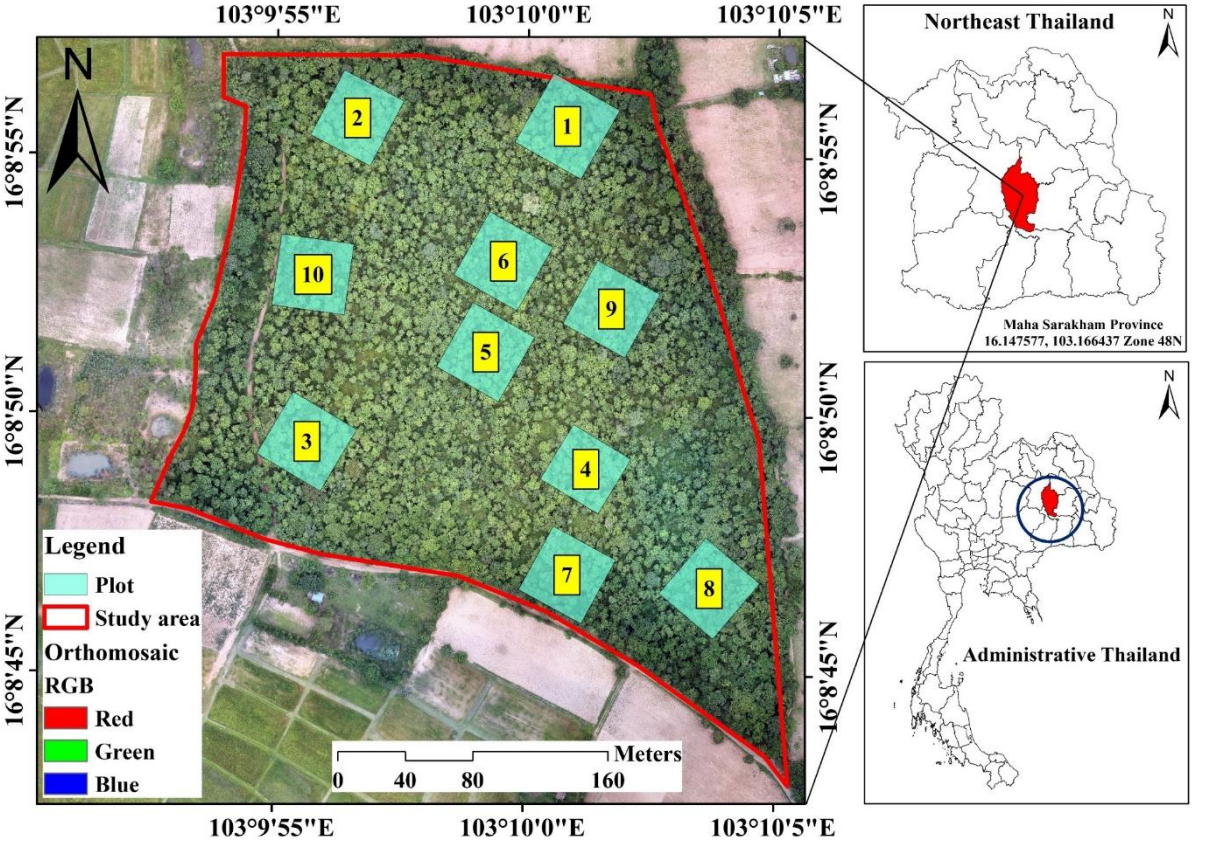

Fig. 1: The study area and ten sample plots, each 40 × 40 meters.

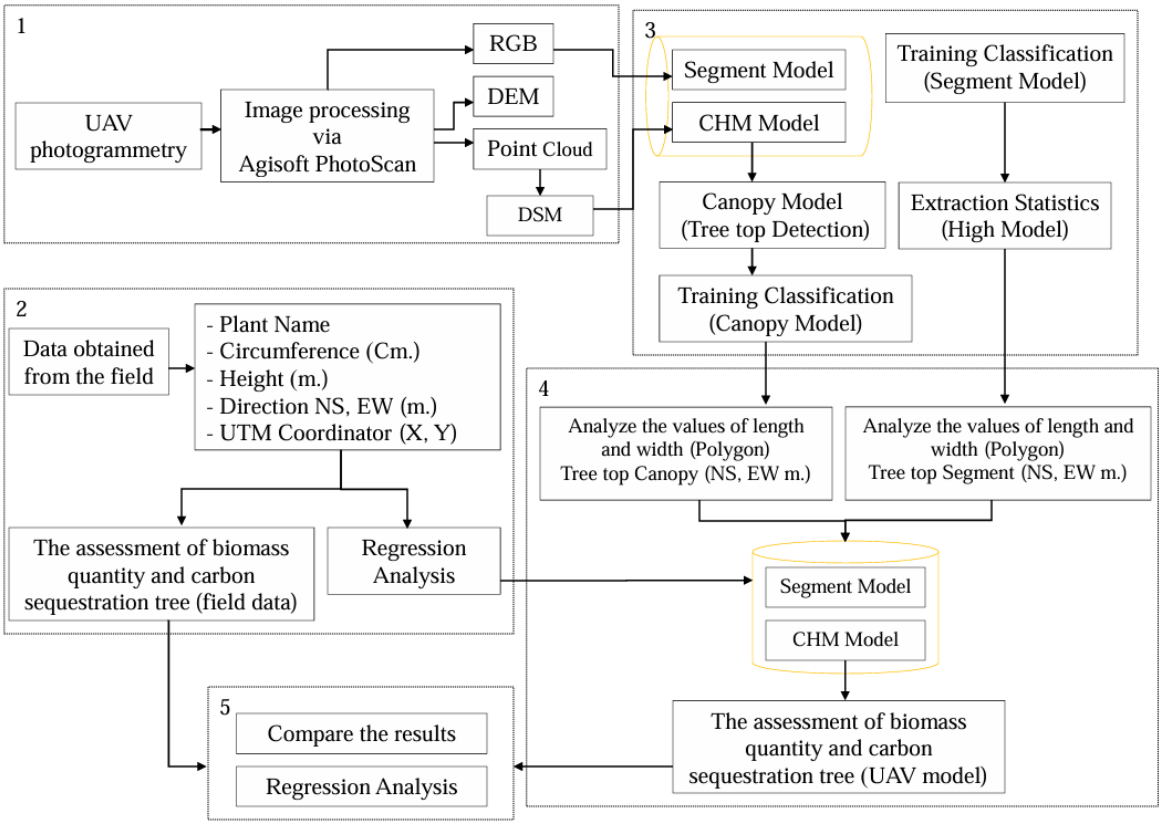

Fig. 2: Workflow for estimating biomass and carbon sequestration using UAV imagery and field data integration.

This community forest is classified as a dry dipterocarp forest, covering approximately 10.66 hectares, situated at an average elevation of 200 meters above sea level. The physical characteristics of the forest consist of a plateau without mountains, resulting in relatively mild heat during summer and cool temperatures in winter. The average annual temperature of this area is 27.40 °C, with an average minimum temperature of 22.40 °C and an average maximum temperature of 33.70 °C. The surrounding community utilizes the forest's resources for various livelihoods, including collecting mushrooms, vegetables, herbs, and fuelwood.[31,32] For this study, ten sample plots of 40×40 meters were established throughout the community forest.

2.2 Data analysis

The data analysis in this study utilized RGB imagery captured by drones and vegetation data obtained from field surveys, combined with two machine learning techniques: Canopy Height Model (CHM) and Segment Mean Shift (SMS).[33-35] The biomass of the trees was calculated by comparing the results obtained from the two machine learning techniques with field survey data. The analysis process is illustrated in Fig. 2 and can be described as follows:

2.2.1 Image processing from drones

This research utilized a DJI Phantom 4 Pro drone equipped with a 20-megapixel camera. For the survey, flight paths were planned at an altitude of 100 m above ground level (Fig. 3). The flight parameters were configured to achieve an 85% overlap in images and a 70% side lap, with the camera's positional accuracy established at 10 meters and a tilt angle precision of 2 degrees. A grid flight path was employed to develop a two-dimensional map. The images obtained were stored in JPG format, featuring a resolution of 5,472 × 3,648 pixels, which resulted in a total of 321 images encompassing the entire survey region. Image processing was performed utilizing Agisoft PhotoScan software. The outcome was a 3D point cloud dataset that depicted the area's location in X, Y, and Z coordinates. This data was subsequently analyzed to produce a Digital Surface Model (DSM), a Digital Elevation Model (DEM), and an Orthophotography.

Fig. 3: UAV flight path design and aerial data acquisition for detailed image-based mapping of the survey area.

2.2.2 Field survey

The field survey in this research involved the following steps and details: 1) The Universal Transverse Mercator (*UTM*) coordinate measurement: To record the position of every tree in the sample plots, we used a Global Positioning System (GPS) device to precisely determine the UTM coordinates of each tree, enabling future tracking and analysis of changes. 2) Tree height measurement: The height of every tree with a size of 15 cm or greater was measured using a Nikon Forestry Pro II rangefinder, a device equipped with laser technology to ensure accuracy and reliability in measurements. 3) Diameter at breast height measurement: The diameter at breast height (DBH) of each tree was measured at approximately 1.30 meters above ground using a standard measuring tape, a critical step for estimating the biomass of the trees. Additionally, the sample plots in this research consisted of ten plots, each measuring 40 × 40 meters, accounting for 10% of the total research area. A random sampling method was used to select the locations of the sample plots. Due to the limitation of not being able to measure the DBH of trees outside the sample plots, this research developed parameters for analysis using regression analysis Eqs. (1) and (2),[36] allowing for reasonable and systematic prediction and evaluation of the characteristics of trees outside the sample plots.

$$y = \beta_1 x_1 + \beta_2 x_2 + \beta_3 x_3 + \varepsilon \tag{1}$$

where y represents the estimation of the DBH, β denotes the coefficients used in the estimation process, which are assigned specific values, x_1 indicates the value of North and South (NS), referring to the canopy height, x_2 signifies the value of East and West (EW), also related to the canopy height, x_3 refers to the value of High tree, which pertains to the canopy height, ε is the constant value used in the calculations.

$$y = (-16.292) + (6.633 * X1) + (5.915 * X2) + (2.038 * X3) \tag{2}$$

2.3 Construction of machine learning regression models

2.3.1 Canopy height model (CHM)

The construction of regression models for tree growth prediction using the CHM method involves a complex process that can be explained step-by-step as follows: Initially, canopy models of trees in the study area were created using drone data. This data was converted into a CHM by calculating the difference between the DSM and the DEM. The results of this calculation provide the height of objects on the Earth's surface. This analysis employs Eq. (3),[37-39] a critical tool for height computation. Next, the canopy structures were analyzed using classification techniques. Training samples were created, dividing canopy types into three main categories: (1) visually interpretable canopies, (2) low-density canopies, and (3) roads or open areas. Finally, data was analyzed and processed using the Support Vector Machine (SVM) classifier technique to create classified canopy type files. The classified raster data was then analyzed to calculate the width and length of the central points of polygons using the Minimum Bounding Geometry tool, which created polygons representing the boundaries. The results of this analysis were compared with canopy direction models (NE, EW) in meters. The canopy height data from each polygon was analyzed within the study area to obtain more precise and detailed insights.

$$CHM = DSM - DEM \tag{3}$$

2.3.2 Segment mean shift (SMS)

The construction of machine learning regression models using the SMS method begins with analyzing RGB imagery obtained from drones. A raster dataset was divided into segments to analyze spectral details at a level of 20 and spatial details at a level of 20, quantified in pixels, in order to correspond with the attributes of RGB images captured by drones. Training samples were prepared for learning and data classification, categorizing tree canopy structures into three main types: (1) visually interpretable tree canopies, (2) low-density tree canopies, and (3) roads or open areas. These classification results were further analyzed using the Train Support Vector Machine Classifier technique to create a file for tree canopy classification. After classification, the data were used for Classify Raster analysis, and the width and length of the central points of polygons were calculated using the Minimum Bounding Geometry tool, creating polygons that represented geometric boundary shapes. The results were compared with canopy shape models in various directions (*e.g.*, NE, EW) measured in meters (m). In the final step, the height data of each polygon within the study area was analyzed using the CHM. The average height was extracted using the Spatial Analysis Tool, which employed the Zonal Statistics tool to ensure accurate and reliable height data.

2.4 Above-ground carbon analysis

The analysis of carbon storage in trees is a critical process for understanding the impact of forests on climate change. The calculation of carbon stored in trees is typically performed by measuring the above-ground biomass of the trees. This research utilized data from 10 sample plots selected for the study. The calculation of tree biomass employed the Allometry Equation, which allows for the estimation of biomass based on the size and physical characteristics of trees. For the dry dipterocarp forest studied, the equation developed by Ogawa *et al*., represented by Eqs. (4) and (5) were applied.[18] This equation expresses the relationship between biomass and the diameter at breast height (1.30 meters) and tree height, which are key factors in evaluating carbon storage capacity. To improve the accuracy of the analysis, the CHM and SMS machine learning methods were applied, enabling more precise and efficient carbon storage estimations in trees.

$$W_s = 0.0396 DBH^2 H_t^{0.9326}$$
$$W_b = 0.0348 DBH^2 H_t^{1.0270} \quad (4)$$
$$W_l = \left[\frac{28}{(W_s + W_b + 0.025)^{-1}} \right]$$

$$W_{ct} = W_s + W_b + W_l \quad (5)$$

where D is the diameter at breast height (measured in centimeters), H is the tree height (in meters), and Ws, Wb, and Wl represent the biomass of the stem, branches, and leaves, respectively (all measured in tons per hectare). The total above-ground biomass was transformed into carbon sequestration by applying a multiplication factor of 0.47, as indicated in Eq. (6),[40] which represents the default carbon fraction established by the IPCC.

$$C_j = W_{ct} * FC \quad (6)$$

where Cj represents the carbon storage capacity of a tree (measured in kilograms), Wct denotes the above-ground biomass of the tree (also in kilograms), and FC (set at 0.47) indicates the ratio of carbon quantity to the tree's biomass.

2.5 Model performance evaluation

Evaluating the performance of the models after training is crucial for assessing the quality of predictions. The evaluation typically considers three main parameters: Precision, Recall, and F1-Score, along with Accuracy and error measures such as Mean Absolute Error (MAE) and Root Mean Squared Error (RMSE).[41] These parameters are described as follows:[42,43] 1. Precision: Precision measures the accuracy of predictions by comparing the number of correct predictions (True Positive, TP) to the total number of predictions (including False Positive, FP) and can be calculated using Eq. (7). 2. Recall: Recall indicates the ability to correctly identify annotated samples compared to all annotations that should be predicted and can be calculated using Eq. (8), where FN represents False Negatives. 3. F1-Score: F1-Score evaluates the balance between Precision and Recall and is calculated using Eq. (9). 4. Accuracy: Accuracy represents the proportion of correct predictions compared to the total number of samples and can be calculated using Eq. (10), where TN represents True Negatives. 5. Error Metrics: To enhance model evaluation accuracy, Mean Absolute Error (MAE) and Root Mean Squared Error (RMSE) are necessary. These are calculated using Eqs. (11) and (12),[44] where MAE measures the average difference between predicted and actual values, and RMSE evaluates the deviation of predictions compared to actual values as the root of the mean squared differences.

$$\text{Precision} = \frac{TP}{TP + FP} \quad (7)$$

$$\text{Recall} = \frac{TP}{TP + FN} \quad (8)$$

$$F1\_Score = \frac{2PR}{P + R} \quad (9)$$

$$Accuracy = \frac{TP}{TP + FN + FP} \quad (10)$$

where TP, or True Positives, represents the number of trees that were correctly identified. FP, or False Positives, indicates the number of trees that were incorrectly identified. FN, or False Negatives, represents the number of trees that were not identified.

$$MAE = \frac{1}{n} \sum_{i=1}^{n} \left| y_1 - y_i \right| \quad (11)$$

where n is the number of observations, y_i is the true value, and $\hat{y}_i$ is the predicted value.

$$RMSE = \sqrt{\sum_{i=1}^{n} \frac{\left(y_i - y_i \right)^2}{n}} \quad (12)$$

From the obtained values, if the MAE and RMSE are low, it indicates that the predicted values are close to the actual values, meaning the model has high prediction accuracy.

3. Results and discussion

The results and discussion of this research on estimating carbon sequestration in community forests using machine learning techniques and remote sensing through drones can be described.

3.1 Results of drones data analysis

The results of carbon storage analysis in the study area are illustrated in Fig. 4. In Fig. 4(a), the DSM results depict the overall characteristics of natural features and man-made structures above ground, including tree canopies in the study area. The study found that height values range from 181.19 to 227.34 meters above sea level. White areas: These represent the highest points at 227.34 meters above sea level. Field surveys identified these areas as having tall tree canopies, clearly revealing surface cover. Brown areas: These areas are densely covered with vegetation, with an average height of 204.26 meters above sea level, indicating a diverse variety of plant species. Orange areas: Field surveys showed these areas have vegetation approximately 1 to 2 meters above the ground, categorized as tree canopies. Green areas: These areas have an elevation of 181.19 meters above sea level and are characterized as low-lying ground covered with surface vegetation. Fig. 4(b) The DEM results represent the Earth's surface without any structures. The elevation within the study area varies between 183.47 and 217.77 meters above sea level. White areas: These are located at 217.77 meters above sea level, characterized by dense vegetation and high forest richness. Brown areas: These are located at 198.18 meters above sea level and are characterized by a diverse range of plant species. Orange areas: Field surveys revealed vegetation 1 to 2 meters high, categorized as tree canopies. Green areas:

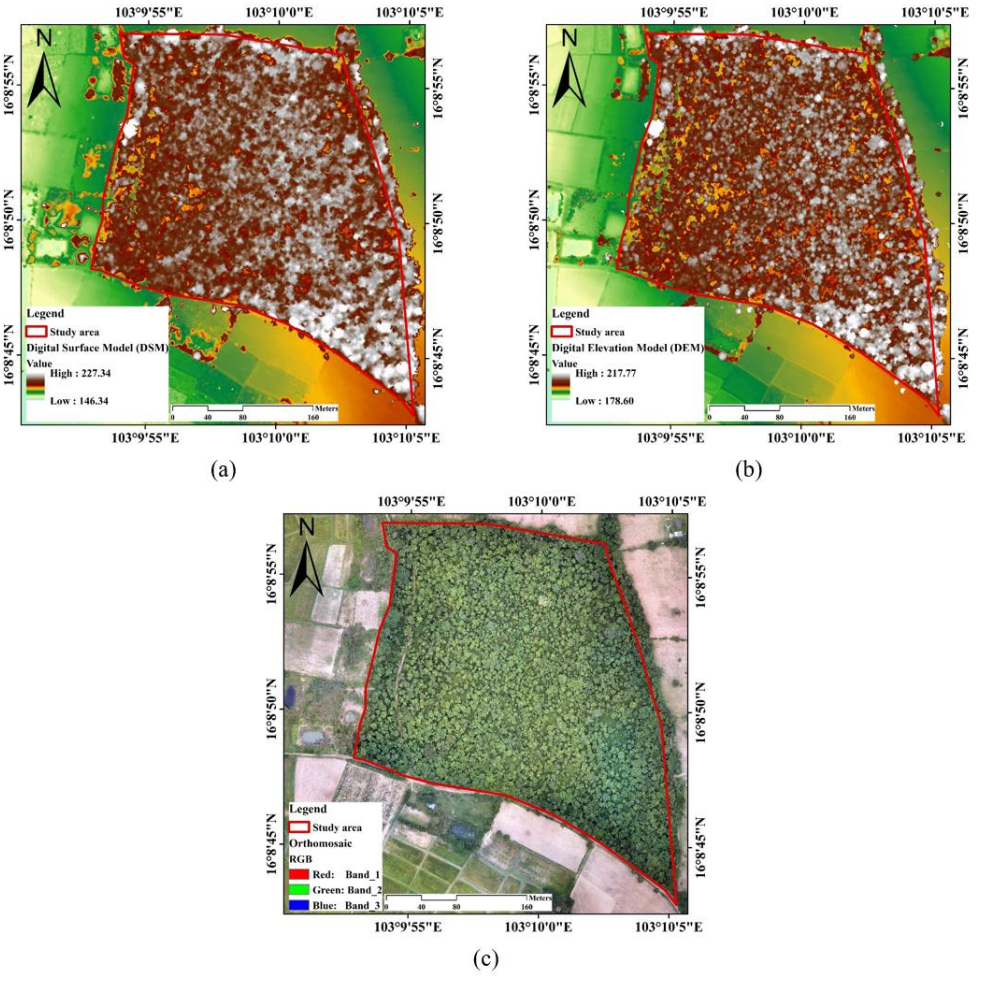

Fig. 4: Drones data analysis (a) DSM, (b) DEM, and (c) Orthophoto (RGB Image).

These areas are at 183.47 meters above sea level, representing water flow paths, such as those formed by rainfall or human activity.

Fig. 4(c) The orthophoto consists of red (R), green (G), and blue (B) bands, enhancing the clarity of aerial drone images. These images were corrected using orthorectification processes to eliminate distortions caused by terrain elevation differences and camera tilt, using terrain height data and referencing the UTM grid system. The resulting images are precise in position, size, and shape, allowing for accurate distance measurement. The high-quality images obtained in a short time can be applied to various machine learning model analyses.

3.2 Results of field data survey

The field survey results from all sample plots revealed 22 families and 39 species. The three most abundant families were FABACEAE with 475 trees, DIPTEROCARPACAE with 291 trees, and RUBIACEAE with 117 trees, while the three least abundant families were BIGNINIACEAE, CELASTRACEAE, and LEGUMINOSAE, each represented by only one tree. A total of 1,241 trees were recorded across the 10 sample plots, with an average of 124 trees per plot. The top 10 most abundant species are presented in Table 1.

Table 1: The field survey results from all sample plots.

No.	Scientific Name	Quantity
1	*Xylia xylocarpa* (Roxb.) Taub.	457
2	*Shorea obtusa Wall*. ex Blume	224
3	*Memecylon edule* Roxb.	56
4	*Lannea coromandelica* (Houtt.) Merr.	56
5	*Hymenopyramis parvifolia* Moldenke	54
6	*Buchanania* lanzan	40
7	*Shorea siamensis* Miq.	40
8	*Morinda elliptica* (Hook.f.) Ridl.	34
9	*Catunaregam tomentosa* (Blume ex C.) Triveng	26
10	*Gardenia obtusifolia* Roxb. ex Hook. f.	23

In this research, since the number of trees outside the sample plots could not be determined, a regression analysis was conducted to analyze the relationship between the diameter at breast height (DBH, cm), tree height (H, m), and

canopy dimensions (NE, EW, m). The field data analysis results are summarized in Table 2. As shown in Table 2, the regression analysis results demonstrate a significant relationship between DBH and tree height, as well as canopy direction. The coefficient of determination (R^2) is 0.654660703, indicating a strong correlation between the datasets. Furthermore, the analysis reveals that as trees grow, their DBH expands in proportion to their height and branch development, which increases the canopy width on average.

Table 2: The regression analysis.

Regression statistics	
Multiple R	0.809111057
R Square	0.654660703
Adjusted R Square	0.653823178
Standard Error	12.35636358
Observations	1241

This relationship is crucial for data analysis and model prediction, especially for estimating the characteristics of trees outside the sample plots. The regression model's constants are essential for analyzing the relationships between variables such as DBH, tree height, and canopy direction. These coefficients help predict and explain tree growth. The regression coefficient analysis results are shown in Table 3. In Table 3 indicates that the regression coefficient intercept is -16.27656375, reflecting the relationship between the dependent variable and the three independent variables in the context of linear regression modeling to describe positive correlations among DBH, tree height (H), and canopy dimensions (NE, EW). The standard error of 1.307552208 serves as a measure of the deviation of the mean from the variables, reflecting the level of data dispersion. A low standard error indicates high precision in the estimated intercept and the generated regression equation. The relationship equation and AGB estimation used a linear regression equation as expressed in Eq. (1) to describe the relationship between DBH, H, and canopy data. This equation was developed from machine learning within the Tree-Tops Detection model of the Canopy and Segmentation methods. All variables demonstrated positive correlations, consistent with the model results.

Table 3: The regression coefficient analysis results.

	Coefficients	Standard Error
Intercept	-16.27656375	1.307552208
NS	6.636432338	0.435307307
EW	5.908540477	0.572480462
High tree	2.039210137	0.190307565

Overall, the analysis produced graphs derived from intercept points to illustrate the connections among the variables. These graphs align with the regression equations developed from the model analysis, as shown in Fig. 5.

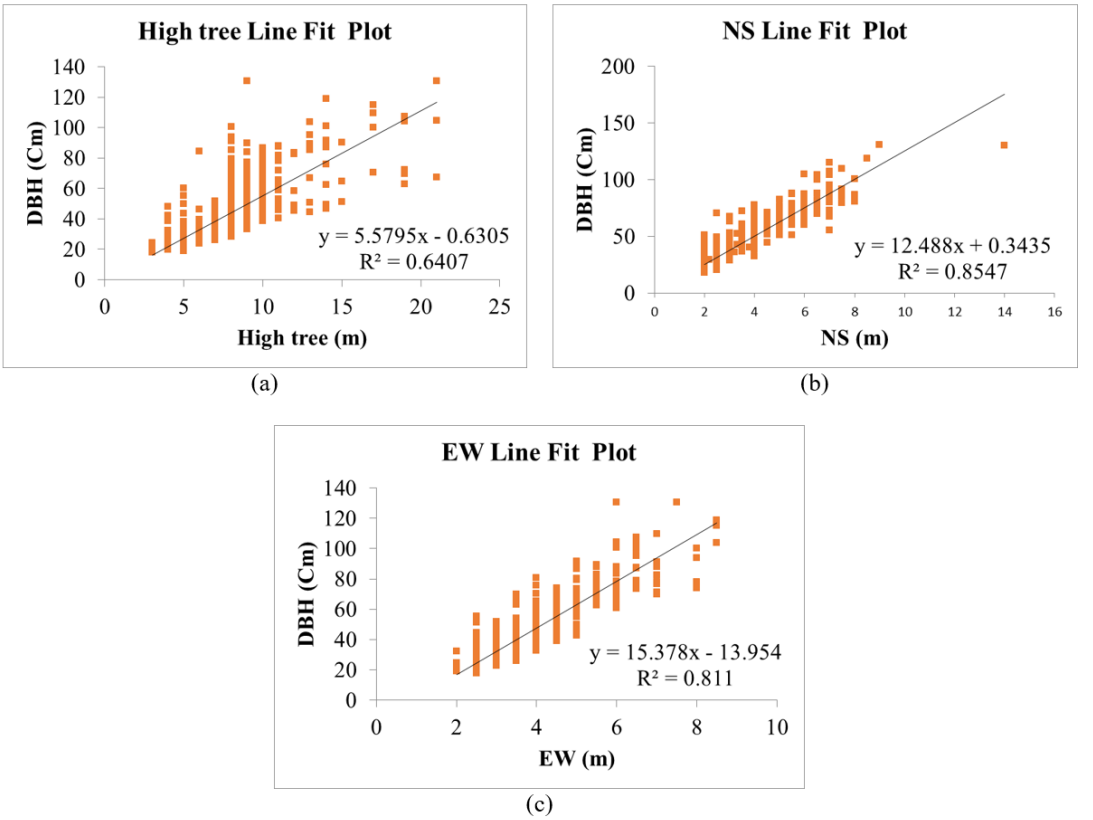

Fig. 5: The regression analysis (a) The relationship between DBH and tree height from analyzed field data, (b) The relationship between DBH and the north-south (NS) canopy, and (c) The relationship between DBH and the east-west (EW) canopy.

Fig. 5(a) The relationship between diameter at breast height (DBH) and tree height from analyzed field data shows a correlation coefficient (R^2) of 0.6406, indicating a moderate to high positive correlation. This positive correlation implies that as the DBH of a tree increases, the tree height tends to increase proportionally. Tree growth is interrelated both vertically (height) and horizontally (DBH). Generally, trees with larger trunks tend to grow taller due to biological factors and the simultaneous accumulation of biomass. This observed relationship reflects the natural growth patterns of trees, and the data can be used to enhance the accuracy of carbon stock studies, which are essential for effective forest resource management planning. Additionally, this analysis provides valuable information on tree growth and biomass accumulation. However, while the R^2 value of 0.6406 indicates a moderate to high correlation, there is still unexplained variance. Future studies should explore additional factors, such as environmental and climatic conditions, to obtain more comprehensive and accurate data for forest resource management.

Fig. 5(b) The relationship between DBH and the north-south (NS) canopy expansion direction reveals a correlation coefficient (R^2) of 0.8547, indicating a strong positive correlation. This means that as the DBH of a tree increases, the size of its canopy in the north-south direction also tends to expand. This expansion is a natural result of tree growth, where an increase in DBH due to biomass accumulation corresponds with a simultaneous expansion of the canopy in the NS direction. A wider canopy allows the tree to capture more sunlight, enhancing photosynthesis efficiency. Canopy growth in these two directions typically occurs in balance, reflecting the proportional accumulation of biomass in the trunk and branches. This analysis reveals a clear relationship between DBH and north-south canopy expansion, with a high correlation coefficient ($R^2 = 0.8547$) indicating significant and reliable data. Furthermore, understanding the growth relationship between DBH and canopy expansion aids in comprehending the natural mechanisms of biomass accumulation and the efficient use of sunlight. This information is valuable for forestry research and the sustainable management of natural resources.

Fig. 5(c) The relationship between DBH and the east-west (EW) canopy direction shows a correlation coefficient (R^2) of 0.8111, indicating a high and positive correlation. This suggests that as the DBH of a tree increases, the size of its canopy in the east-west direction also tends to expand. This relationship reflects the growth patterns of trees in both horizontal (canopy) and vertical (trunk) directions, which are consistent and balanced due to the photosynthetic process. Particularly in areas with adequate sunlight, the expansion of the canopy in the east-west direction indicates the tree's response to environmental factors such as wind direction, sunlight availability, and open space for branch growth. This analysis highlights the importance of observing and analyzing factors that influence tree growth. The positive correlation indicates the tree's ability to adapt and expand in directions favorable for sunlight and wind utilization. This information is useful for planning and caring for trees in various areas. However, future studies should consider other factors, such as soil and water conditions, to provide a more comprehensive overview.

3.3 Results of machine learning model development

The results of developing machine learning models using drone-collected data on the physical characteristics of trees, such as canopy shape, canopy size, and height, are shown in Fig. 6. In Fig. 6(a), the CHM analysis results from drone data were transformed into high-resolution spatial models using Spatial-Spectral Analysis, which represented tree canopies as polygons with coordinates and heights. A total of 123,555 polygons were detected, each representing a visible tree canopy within the analyzed area. The study analyzed canopy

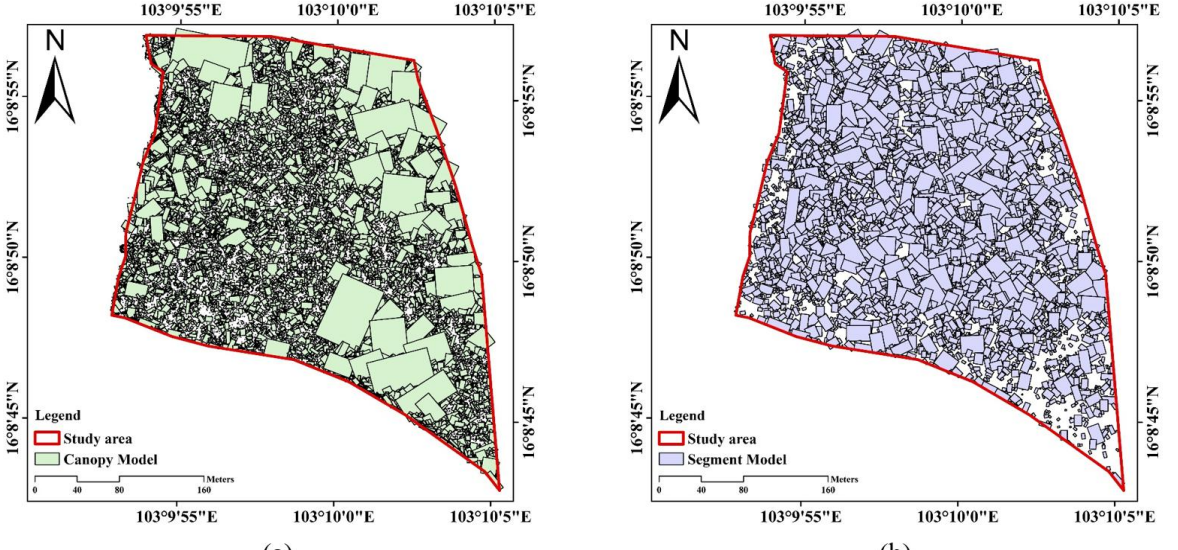

Fig. 6: (a) The CHM analysis result, and (b) the SMS analysis result.

structures using classification techniques and calculated the width and length of the central points of the polygons. The average height of tree polygons was 5 meters, reflecting the median growth level of trees in the area. The canopy size in the north-south direction (NS) averaged 0.77 cm, representing the vertical extent (N-S) of the canopies, while the canopy size in the east-west direction (EW) averaged 0.42 cm, indicating the horizontal extent (E-W). The DBH averaged 15 cm, reflecting the trunk growth rate at breast height.

In Fig. 6(b), the SMS analysis employed a clustering technique to group pixels in the images with similar spectral characteristics, effectively segmenting tree shapes or parts. This resulted in 5,165 polygons, reflecting the number of trees or parts. The polygon analysis of the tree layers revealed an average height (H) of 6 meters, indicating smaller trees detected using this technique, which may include young trees or those in dense areas. The canopy size in the north-south direction (NS) averaged 3 meters, reflecting the horizontal growth dimension of the trees. In contrast, the canopy size in the east-west direction (EW) averaged 0.42 meters, indicating relatively small canopy expansion in this direction, possibly due to limited growth or environmental constraints. The DBH averaged 50 cm, indicating the trunk diameter at breast height, which reflects the mature tree's dimensions.

3.4 Results of accuracy analysis

The accuracy analysis between field data and the results from the two canopy model analyses was conducted with a height threshold set at 3 meters above ground level to ensure consistency with field data. The accuracy analysis results are shown in Table 4.

Table 4: Model canopy analysis results.

Canopy analysis results		Tree canopy (sq.m.)	
		CHM (m^2)	SMS (m^2)
True Positive	TP	24,423.84	38,350.17
False Negative	FP	2,639.37	41,427.18
False Positive	FN	13,872.39	28,546.43

From Table 4, it is evident that the canopy models developed using drone data demonstrate excellent agreement with field data. This analysis employed a comparison between the model results and ground truth data collected from field surveys, using the intersection technique to identify overlapping areas between the two layers and thereby verify the accuracy of the canopy models (Table 5). The results highlight the high accuracy of canopy model processing compared to field data. The use of drone data enhanced analysis efficiency by enabling comprehensive and detailed data collection. However, model development requires ongoing validation and refinement to address the complexities of data in different environmental conditions. Overall, this effort is considered successful in utilizing technology to improve the accuracy of geographic data analysis.

Table 5: The accuracy of the canopy and segment models.

ID	CHM	SMS
Precision	0.902	0.481
Recall	0.638	0.573
Accuracy	0.597	0.354
F1-Score	0.747	0.523
Percent	74.737%	52.293%

From the analysis results presented in Table 5, the performance of the two models, CHM and SMS, was evaluated using metrics such as Precision, Recall, Accuracy, F1-Score, and Percent. The CHM model demonstrated strong performance in accurately classifying tree canopy shapes, efficiently identifying trees or canopies from field data, with an F1-Score of 0.747 or 74.737%, indicating high overall accuracy in simulating tree canopies. In contrast, the SMS model showed lower performance compared to CHM. Its capability to analyze and detect trees or canopies was relatively limited, resulting in higher overall errors. The combination of Precision and Recall for this model resulted in an F1-Score of 0.523 or 52.3%, reflecting lower accuracy and balance compared to the CHM in predicting tree canopies.

3.5 Results of regression analysis

The regression analysis of carbon density relationships compared field data with estimated carbon density derived from drones using machine learning methods to examine quantitative relationships across 10 sample plots. The results showed a correlation between field data and drone-based estimates in 5 sample plots, reflecting data consistency and providing opportunities to improve the model for higher accuracy. The overall R^2 value was 0.690163471 or 69%, as shown in Table 6, indicating a moderate level of correlation. These results were used to create graphs that align with equations generated from model analysis, as shown in Fig. 7.

Table 6. Regression statistics results.

Regression Statistics	
Multiple R	0.830760778
R Square	0.690163471
Adjusted R Square	0.380326941
Standard Error	0.729496444
Observations	5

The relationships are visualized in graphs in Fig. 7. Fig. 7(a) illustrates the relationship between above-ground biomass estimates from the CHM machine learning method, derived from DEM and DSM analysis of RGB imagery of tree canopies in community forests, with an R^2 value of 0.9895 or

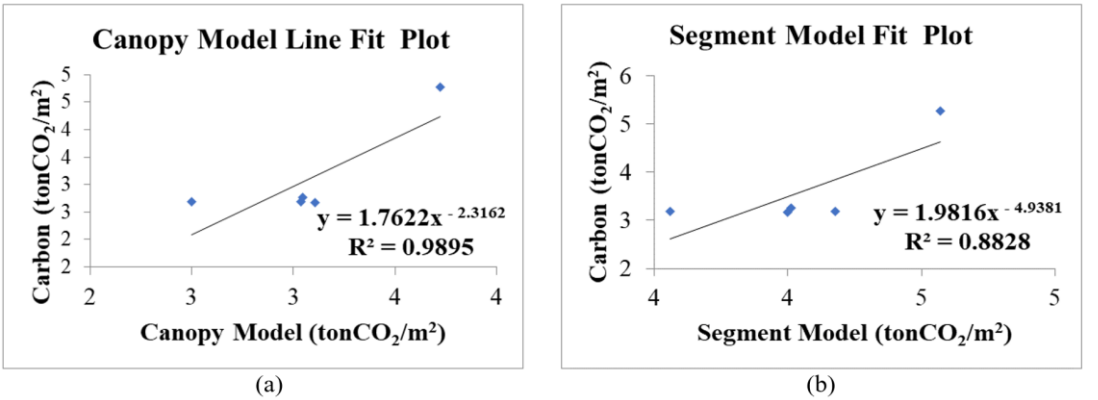

(a) (b)

Fig. 7: Regression analysis (a) illustrates the relationship between above-ground biomass estimates from the CHM, and (b) illustrates the relationship between above-ground biomass estimates from the SMS.

y = 1.7622x-2.3162, indicating stronger correlations than SMS. Fig. 7(b) illustrates the relationship between above-ground biomass estimates from the SMS machine learning method, derived from RGB imagery of tree canopies in community forests, with an R^2 value of 0.8828 or y = 1.9816x -4.9381, indicating weaker correlations compared to CHM. The coefficients of the model represent numerical values that aid in optimizing the model's performance, as shown in Table 7. The remaining 5 plots with weaker correlations highlight model limitations, such as insufficient data, inconsistent areas, or environmental factors not accounted for in the model, including environmental differences or data errors. From the coefficients in Table 7, the CHM model's coefficients for independent variables show positive relationships with dependent variables, while the SMS model shows negative coefficients, indicating opposite directions.

The standard error helps evaluate uncertainty in coefficient estimates, with lower values indicating higher accuracy, as shown in Table 7. In Table 8, the regression analysis results of both models for carbon storage estimation highlight critical metrics such as Correlation Coefficient, MAE, and RMSE to evaluate model relationships and accuracy. The analysis found that CHM achieved a correlation coefficient of 0.9895, demonstrating higher prediction accuracy than SMS, which had a Correlation Coefficient of 0.8828. Moreover, CHM's MAE was 0.4624, and its RMSE was 0.5538, both of which were significantly lower than SMS's MAE of 1.0285 and RMSE of 1.1270, clearly indicating CHM's superior accuracy and reliability.

Table 7: The outcomes of the coefficients.

	Coefficients	Standard Error
Intercept	-0.94016861	6.871139141
Segment	-0.885798185	4.09203767
Canopy	2.483713486	3.437145602

Table 8: Regression analysis model.

Summary	Regression Analysis Model	
	CHM	SMS
Correlation coefficient	0.9895	0.8828
Mean absolute error	0.4624	1.0285
Root mean squared error	0.5538	1.1270

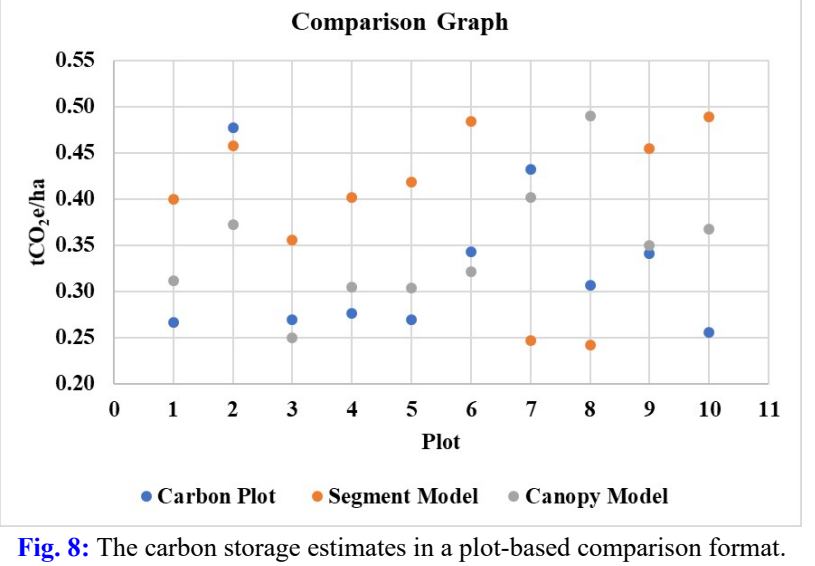

Fig. 8: The carbon storage estimates in a plot-based comparison format.

Table 9: Above-ground carbon sequestration results.

Carbon sequestration		Plant component	Biomass quantity		Carbon sequestration capacity		Carbon sequestration capacity (kg/ha)	Percentage proportion
			Average (tCO_2e/ha)	Per area ($kgCO_2e/m^2$)	Average (tCO_2e/ha)	Per area ($kgCO_2e/m^2$)		
Field data	Plant part	Stem	0.000311	3.106160	0.022120	1.459895	0.000146	24.35
		leave	0.000105	1.047605	0.007460	0.492374	0.492374	8.21
		branch	0.000015	0.148418	0.001057	0.069756	0.069756	1.16
Machine learning	CHM	Stem	0.000326	3.258323	0.023203	1.531412	1.531412	25.55
		leave	0.000088	0.875185	0.006232	0.411337	0.411337	6.86
		branch	0.000015	0.148285	0.001056	0.069694	0.069694	1.16
	SMS	Stem	0.000295	2.947583	0.020990	1.385364	1.385364	23.11
		leave	0.000108	1.079388	0.007687	0.507313	0.507313	8.46
		branch	0.000014	0.143864	0.001024	0.067616	0.067616	1.13
total			0.001275	12.754811	0.090830	5.994761	4.535012	100

3.6 Above-ground carbon analysis

The analysis of above-ground carbon using machine learning techniques combined with the Allometry Equation estimated tree biomass and carbon storage in the study area. The biomass and carbon content calculations were based on the physical characteristics of the trees, including DBH, tree height, and species type. By applying machine learning techniques to analyze biomass and carbon, the accuracy of spatial data assessment was improved. The evaluation results for three methods—Field Data, CHM, and SMS—are presented in Table 9.

The error analysis of carbon storage per area from the CHM and SMS models is shown in Table 10 as percentages. The errors for the two models were -0.48% and -3.15%, with differences in total carbon storage of 1.01 and 6.52 tonCO_2e, respectively. Additionally, the carbon storage estimates in a plot-based comparison format from ten plots of 40 × 40 meters, as shown in Fig. 8, illustrate the relationships between plots and reveal clear data trends.

3.7 Results of carbon density analysis

The results of carbon density analysis are presented in Table 9.

Table 10: Results of the analysis of carbon sequestration error per area.

Carbon Sequestration	Carbon density per area (field data)	Machine learning Carbon Sequestration	
		CHM	SMS
tCO_2e	213.53	212.51	207.01
$kgCO_2e/m^2$	2.022026	2.012442	1.960293
tCO_2e/ha	0.002022	0.000201	0.000196
Error (%)	-	0.48%	3.15%
Carbon sequestration total quantity difference carbon density per area ($kgCO_2e$)		0.001020	0.006520

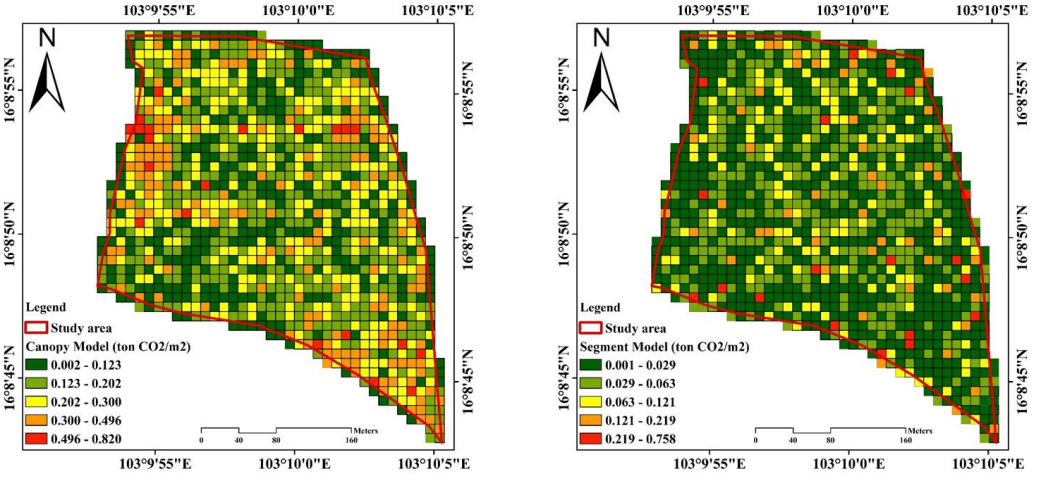

(a) (b)

Fig. 9: Carbon density analysis (a) carbon density per unit area as determined by CHM, and (b) carbon density per unit area as assessed by SMS.

The study applied the Allometric Equation to analyze the spatial distribution of carbon density using CHM and SMS in polygonal units, with a 10 square meter (0.001 hectare) subarea as the analysis unit. This approach enabled a more detailed and specific understanding of carbon distribution. The results are illustrated in Fig. 9. Fig. 9(a) shows the carbon density per area using CHM. The study found that the carbon density in rectangular polygons of 10 square meters or 0.001 hectares ranged from 0.0 to 0.820 tonCO_2eq/m². Areas with the highest density, marked in red, ranged from 0.496 to 0.820 tonCO_2eq/m² and were characterized by dense vegetation, as indicated by canopy modeling and tree height data from drones, which showed high canopy cover and strong DBH relationships. The lowest carbon density areas, marked in green, ranged from 0.000 to 0.123 tonCO_2eq/m². These areas had sparse canopy cover, smaller DBH values (below 15 cm), and were dominated by undergrowth. The average carbon density in these areas was 0.0625 tonCO_2eq/m² or 0.01 t/ha.

Fig. 9(b) shows the carbon density per area using SMS. The study found that the carbon density in rectangular polygons of 10 square meters or 0.001 hectares ranged from 0.001 to 0.785 tonCO_2eq/m². Areas with the highest density, marked in red, ranged from 0.129 to 0.785 tonCO_2eq/m² and were characterized by dense vegetation, as indicated by canopy modeling and tree height data from drones, which showed high canopy cover and strong DBH relationships. The lowest carbon density areas, marked in green, ranged from 0.001 to 0.029 tonCO_2eq/m². These areas had sparse canopy cover, smaller DBH values (below 15 cm), and were dominated by undergrowth. The average carbon density in these areas was 0.393 tonCO_2eq/m² or 0.05502 t/ha.

The findings of this research are consistent with those of Tian *et al.*[45] and Chen *et al.*,[46] which utilize the concepts of CHM and SMS in assessing carbon density in forest areas that can be further developed for future research. This includes the development of more accurate models such as the Canopy Height Layer-Biomass Estimation Model (CHL-BEM), which uses full-waveform LiDAR data combined with Machine Learning and Deep Learning to precisely separate canopy layers. Moreover, integrating data from drones and Hyperspectral Imaging is recommended to enhance the accuracy of canopy classification and carbon assessment. The use of AI to analyze forest data and adapt models to suit different areas, as well as studying the long-term impact of climate conditions on canopy structure and biomass, is also recommended. Additionally, this research methodology can be applied in conservation and environmental policy areas, such as calculating carbon credits and setting conservation area boundaries. These approaches support the effective formulation of environmental policies.

4. Conclusion

The emission of greenhouse gases, such as carbon dioxide, is a primary cause of global temperature rise. Expanding forested areas and absorbing carbon through trees are vital solutions to this issue. Our research area is situated in a community forest in Maha Sarakham Province, spanning approximately 10.56 hectares and featuring a diverse array of tree species. In this study, drone technology was used to capture RGB imagery, which was analyzed using Agisoft PhotoScan software. Additionally, field measurements of trees were conducted to compare with those obtained from drone imagery. The study employed machine learning models, CHM and SMS, to detect tree canopies and calculate above-ground biomass. The average carbon storage from field data, CHM, and SMS was approximately 0.002025, 0.0020125, and 0.00196875 tCO_2e/m², respectively. Using a Regression Analysis Model to evaluate the relationships and accuracy of the two models, CHM showed a Correlation Coefficient (R) of 0.9895, indicating high efficiency, along with low MAE and RMSE values, reflecting minimal prediction errors. Thus, the use of drones and machine learning techniques demonstrates an

effective method for carbon estimation and holds significant potential for sustainable community forest management in the future.

Acknowledgments
This research project is financially supported by Mahasarakham University.

Conflict of Interest
There is no conflict of interest.

Supporting Information
Not applicable.

References
[1] M. Filonchyk, M. P. Peterson, L. Zhang, V. Hurynovich, Y. He, Greenhouse gases emissions and global climate change: Examining the influence of CO_2, CH_4, and N_2O, *Science of The Total Environment*, 2024, **935**, 173359, doi: 10.1016/j.scitotenv.2024.173359.
[2] C. Le Quéré, R. Jackson, M. B. Jones, W. A. Andreev, D. C. E. Bakker, Z. Barcza, S. Zaehle, Global Carbon Budget 2022, *Earth System Science Data*, 2022, **14**, 2671-2740, doi: 10.5194/essd-14-4811-2022.
[3] L. Liu, B. Li, Z. Chen, J. Liu, Global Warming and Its Impact on Human Health: A Review, *International Journal of Environmental Research and Public Health*, 2022, **19**, 6695, doi: 10.3390/ijerph19116695.
[4] J. Rogelj, D. Shindell, K. Jiang, S. Fifita, P. Forster, V. Ginzburg, D. P. van Vuuren, Pathways limiting global warming to 1.5 °C, *World Meteorological Organization*, 2019, **9**, 713-718, doi: 10.1038/s41558-019-0579-0.
[5] T. Angkahad, T. Laosuwan, S. Sangpradid, N. Prasertsri, Y. Uttaruk, T. Phoophathong, J. Nuchthapho, An empirical analysis of above-ground biomass and carbon sequestration using UAV photogrammetry and machine learning techniques, *IEEE Access*, 2024, **12**, 186740-186752, doi: 10.1109/ACCESS.2024.3514074.
[6] W. Jundang, L. Puangchit, S. Diloksumpun, Carbon storage of dry dipterocarp forest and eucalypt plantation at Mancha Khiri plantation, Warasan Wanasat, *Faculty of Forestry, Kasetsart University*, 2012, **29**, 36-44,
[7] M. Wang, J. Xie, M. Lyu, Forest soil carbon cycle in response to global change, *Forests*, 2023, **14**, 2242, doi: 10.3390/f14112242.
[8] T. Laosuwan, Y. Uttaruk, S. Sangpradid, C. Butthep, S. Leammanee, The carbon sequestration potential of Silky Oak (Grevillea robusta A.cunn. Ex R.br.), a high-value economic wood in Thailand, *Forests*, 2023, **14**, 1824, doi: 10.3390/f14091824
[9] Y. Uttaruk, T. Laosuwan, S. Sangpradid, C. Butthep, T. Rotjanakusol, W. Sittiwong, S. Nilrit, Thailand's urban forestry programs are assisted by calculations of their ecological properties and economic values, *Land*, 2024, **13**, 1440, doi: 10.3390/land13091440.
[10] T. Laosuwan, Y. Uttaruk, T. Rotjanakusol, Atmospheric environment monitoringin Thailand *via* satellite remote sensing: a case study of carbon dioxide, *Polish Journal of Environmental Studies*, 2023, **32**, 3645-3651, doi: 10.15244/pjoes/166170.
[11] Y. Uttaruk, P. V. Khoa, T. Laosuwan, A guideline for greenhouse gas emission reduction and carbon sequestration in forest sector based on Thailand voluntary emission reduction programme, *Sains Malaysiana*, 2024, **53**, 477-486, doi: 10.17576/jsm-2024-5303-01.
[12] T. Laosuwan, Y. Uttaruk, S. Nakapan, J. Itsarawisut, C. Plybour, Evaluation of tree biomass and carbon sequestration through remote sensing and field methods, *Geographia Technica*, 2025, **20**, 33-43, doi: 10.21163/gt_2025.201.04.
[13] Y. Uttaruk, T. Laosuwan, Development of prototype project for carbon storage and greenhouse gas emission reduction from Thailand's agricultural sector, *Sains Malaysiana*, 2019, **48**, 2083-2092, doi: 10.17576/jsm-2019-4810-03.
[14] T. Pothong, S. Elliott, S. Chairuangsri, W. Chanthorn, D. P. Shannon, P. Wangpakapattanawong, New allometric equations for quantifying tree biomass and carbon sequestration in seasonally dry secondary forest in northern Thailand, *New Forests*, 2022, **53**, 17-36, doi: 10.1007/s11056-021-09844-3.
[15] F. Noulèkoun, J. B. Naab, J. P. A. Lamers, S. Baumert, A. Khamzina, Sapling biomass allometry and carbon content in five afforestation species on marginal farmland in semi-arid Benin, *New Forests*, 2018, **49**, 363-382, doi: 10.1007/s11056-017-9624-2.
[16] V. T. Nam, M. van Kuijk, N. P. R. Anten, Allometric equations for aboveground and belowground biomass estimations in an evergreen forest in Vietnam, *PLoS One*, 2016, **11**, e0156827, doi: 10.1371/journal.pone.0156827.
[17] S. Baumert, A. Khamzina, Allometric relations in Jatropha curcas production systems of Burkina Faso, *Journal of Arid Environments*, 2015, **120**, 95-104, doi: 10.1016/j.jaridenv.2015.04.015.
[18]. H. Ogawa, K.Yoda, K. Ogino, T. Kir, Comparative ecological studies on three main type of forest vegetation in Thailand. II. *Structure and floristic composition.: nature & Life in SE Asia*, 1965, **4**, 49-80.
[19] T. S. Chinembiri, O. Mutanga, T. Dube, Landsat-8 and sentinel-2 based prediction of forest plantation C stock using spatially varying coefficient Bayesian hierarchical models, *Remote Sensing*, 2022, **14**, 5676, doi: 10.3390/rs14225676.
[20] B. M. Gramig, J. M. Barnard, L. S. Prokopy, Farmer beliefs about climate change and carbon sequestration incentives, *Climate Research*, 2013, **56**, 157-167, doi: 10.3354/cr01142.
[21] J. D. Watts, R. L. Lawrence, P. Miller, C. Montagne, An analysis of cropland carbon sequestration estimates for North Central Monana, *Climatic Change*, 2011, **108**, 301-331, doi: 10.1007/s10584-010-0009-1.
[22]. P. Saengpradit, S. Sangpradid, T. Laosuwan, Estimation of Above-Ground Biomass using Hybrid Machine Learning based on Satellite Imagery, *International Journal on Technical and Physical Problems of Engineering*, 2024, **16**, 7-13
[23]. W. Vattanavongsiri, S. Sangpradid, W. Chokkuea, T.

Laosuwan, Estimation of Above-Ground Carbon Sequestration in the National Reserved Forest using Vegetation Indices and Gradient Boosting Machine Learning, *International Journal on Technical and Physical Problems of Engineering*, 2024, **16**, 361-366.
[24] Y. Uttaruk, T. Laosuwan, Comparison of carbon storage measurement methods on agroforestry systems in sakon Nakhon Province, northeast Thailand, *Basic and Applied Sciences - Scientific Journal of King Faisal University*, 2020, **21**, 1442, doi: 10.37575/b/sci/2382.
[25] R. Su, W. Du, Y. Shan, H. Ying, R. Wu, R. Li, Aboveground carbon stock estimation based on backpack LiDAR and UAV multispectral imagery at the forest sample plot scale, *Remote Sensing*, 2024, **16**, 3927, doi: 10.3390/rs16213927.
[26] Y. Choi, H. I. Chung, C.-H. Lim, J.-H. Lee, W. I. Choi, S. W. Jeon, Multi-model approaches to the spatialization of tree vitality surveys: constructing a national tree vitality map, *Forests*, 2021, **12**, 1009, doi: 10.3390/f12081009.
[27] A. L. Mitchell, A. Rosenqvist, B. Mora, Current remote sensing approaches to monitoring forest degradation in support of countries measurement, reporting and verification (MRV) systems for REDD, *Carbon Balance and Management*, 2017, **12**, 9, doi: 10.1186/s13021-017-0078-9.
[28] S. Francini, E. Vangi, G. D'Amico, C. Borghi, G. Cencini, C. Monari, C. Zolli, G. Chirici, Field-independent carbon mapping and quantification in forest plantation through remote sensing, *European Journal of Remote Sensing*, 2024, **57**, 2334717, doi: 10.1080/22797254.2024.2334717.
[29] E. P. Y. Chan, T. Fung, F. K. K. Wong, Estimating above-ground biomass of subtropical forest using airborne LiDAR in Hong Kong, *Scientific Reports*, 2021, **11**, 1751, doi: 10.1038/s41598-021-81267-8.
[30] S. J. Goetz, A. Baccini, N. T. Laporte, T. Johns, W. Walker, J. Kellndorfer, R. A. Houghton, M. Sun, Mapping and monitoring carbon stocks with satellite observations: a comparison of methods, *Carbon Balance and Management*, 2009, **4**, 2, doi: 10.1186/1750-0680-4-2.
[31] D. D. Tibuhwa, Wild mushroom: an underutilized healthy food resource and income generator: experience from Tanzania rural areas, *Journal of Ethnobiology and Ethnomedicine*, 2013, **9**, 49, doi: 10.1186/1746-4269-9-49.
[32] M. A. Islam, R. Rai, S. M. S. Quli, Forest resources use for building livelihood resilience in ethnic communities of Jharkhand, *Trends in Biosciences*, 2015, **8**, 1256-1264.
[33] A. Sassu, L. Ghiani, L. Salvati, L. Mercenaro, A. Deidda, F. Gambella, Integrating UAVs and canopy height models in vineyard management: a time-space approach, *Remote Sensing*, 2022, **14**, 130, doi: 10.3390/rs14010130.
[34] G. R. Morgan, C. Wang, J. T. Morris, RGB indices and canopy height modelling for mapping tidal marsh biomass from a small unmanned aerial system, *Remote Sensing*, 2021, **13**, 3406, doi: 10.3390/rs13173406.
[35] W. Yan, H. Guan, L. Cao, Y. Yu, C. Li, J. Lu, A self-adaptive mean shift tree-segmentation method using UAV LiDAR data, *Remote Sensing*, 2020, **12**, 515, doi: 10.3390/rs12030515.
[36] Z. Chen, M. Wang, J. Zhang, Object detection in UAV images based on improved YOLOv5, Cyber Security Intelligence and Analytics, Cham: Springer Nature Switzerland, 2023, 267-278, doi: 10.1007/978-3-031-31775-0_28.
[37] P. Aszkowski, B. Ptak, M. Kraft, D. Pieczyński, P. Drapikowski, Deepness: Deep neural remote sensing plugin for QGIS, *SoftwareX*, 2023, **23**, 101495, doi: 10.1016/j.softx.2023.101495.
[38] G. Chen, Y. Shang, Transformer for tree counting in aerial images, *Remote Sensing*, 2022, **14**, 476, doi: 10.3390/rs14030476.
[39] T. Kattenborn, J. Leitloff, F. Schiefer, S. Hinz, Review on Convolutional Neural Networks (CNN) in vegetation remote sensing, *ISPRS Journal of Photogrammetry and Remote Sensing*, 2021, **173**, 24-49, doi: 10.1016/j.isprsjprs.2020.12.010.
[40] M. Doraisami, G. M. Domke, A. R. Martin, Improving wood carbon fractions for multiscale forest carbon estimation, *Carbon Balance and Management*, 2024, **19**, 25, doi: 10.1186/s13021-024-00272-2.
[41] N. Ahmad, S. Ullah, N. Zhao, F. Mumtaz, A. Ali, A. Ali, A. Tariq, M. Kareem, A. B. Imran, I. A. Khan, M. Shakir, Comparative analysis of remote sensing and geo-statistical techniques to quantify forest biomass, *Forests*, 2023, **14**, 379, doi: 10.3390/f14020379.
[42] C. Wu, F. Zhang, J. Xia, Y. Xu, G. Li, J. Xie, Z. Du, R. Liu, Building damage detection using U-Net with attention mechanism from pre- and post-disaster remote sensing datasets, *Remote Sensing*, 2021, **13**, 905, doi: 10.3390/rs13050905.
[43] R. M. AlZoman, M. J. F. Alenazi, A comparative study of traffic classification techniques for smart city networks, *Sensors*, 2021, **21**, 4677, doi: 10.3390/s21144677.
[44] A. Jierula, S. Wang, T.-M. Oh, P. Wang, Study on accuracy metrics for evaluating the predictions of damage locations in deep piles using artificial neural networks with acoustic emission data, *Applied Sciences*, 2021, **11**, 2314, doi: 10.3390/app11052314.
[45] J. Tian, L. Wang, X. Li, D. Yin, H. Gong, S. Nie, C. Shi, R. Zhong, X. Liu, R. Xu, Canopy height layering biomass estimation model (CHL-BEM) with full-waveform LiDAR, *Remote Sensing*, 2019, **11**, 1446, doi: 10.3390/rs11121446.
[46] X. Chen, Y. Guo, Z. Chen, X. Luo, P. Wang, M. Shi, X. Wang, A new method for estimating forest stand carbon stock: Segmentation and modeling based on forest aboveground imagery, *Ecological Indicators*, 2024, **167**, 112697, doi: 10.1016/j.ecolind.2024.112697.